Intermediate degrees of synergistic pleiotropy drive adaptive evolution in ecological time

Léa Frachon, Cyril Libourel, Romain Villoutreix, Sébastien Carrere, Cédric Glorieux, Carine Huard-Chauveau, Miguel Navascués, Laurène Gay, Renaud Vitalis, Etienne Baron, et al.

Intermediate degrees of synergistic pleiotropy drive adaptive evolution in ecological time

Léa Frachon,[1¶] Cyril Libourel,[1¶] Romain Villoutreix,[2] Sébastien Carrère,[1] Cédric Glorieux,[2] Carine Huard-Chauveau,[1] Miguel Navascués,[3,4] Laurène Gay,[5] Renaud Vitalis,[3,4] Etienne Baron,[2] Laurent Amsellem,[2] Olivier Bouchez,[6,7] Marie Vidal,[6,8] Valérie Le Corre,[9] Dominique Roby,[1] Joy Bergelson,[10] Fabrice Roux[1,2]*

Affiliations :

[1] LIPM, Université de Toulouse, INRA, CNRS, Castanet-Tolosan, France

[2] Laboratoire Evolution, Ecologie et Paléontologie, UMR CNRS 8198, Université de Lille, Villeneuve d'Ascq Cedex, France

[3] INRA, UMR CBGP, F-34988 Montferrier-sur-Lez, France

[4] Institut de Biologie Computationnelle, F- 34095 Montpellier, France

[5] UMR AGAP, INRA, Montpellier, France

[6] INRA, GeT-PlaGe, Genotoul, Castanet-Tolosan, France

[7] GenPhySE, Université de Toulouse, INRA, INPT, INP-ENVT, Castanet Tolosan, France

[8] INRA, UAR1209, Castanet-Tolosan, France

[9] INRA, UMR1347 Agroécologie, France,

[10] Department of Ecology and Evolution, University of Chicago, Chicago, IL USA

[¶] These authors contributed equally to this work.

* To whom correspondence should be addressed. E-mail: fabrice.roux@toulouse.inra.fr

Rapid phenotypic evolution of quantitative traits can occur in natural populations on a timescale of decades or even years[1], but little is known about its underlying genetic architecture[2]. Theoretical investigations have revealed that genes with intermediate pleiotropy will, under certain conditions, drive adaptive evolution[3-4] but these predictions have rarely been tested, especially under ecologically realistic conditions. Here, we performed a resurrection experiment to compare the evolution of multiple traits across six *in situ* micro-habitats within a natural population of the plant *Arabidopsis thaliana*. We then used Genome Wide Association mapping to identify the SNPs associated with evolved and unevolved traits in each of these sites. Finally, a genome-wide analysis of temporal genetic differentiation allowed us to test for selection acting on these SNPs. Phenotypic evolution was consistent across all micro-habitats but GWAS revealed largely distinct genetic bases among sites. Adaptive evolutionary change was largely driven by a small number of QTLs with intermediate degrees of pleiotropy under strong selection; this pleiotropy was synergistic with the per-trait effect size of a SNP increasing with the degree of pleiotropy. In addition to these pleiotropic QTLs, weak selection was detected for frequent small micro-habitat-specific QTLs that shape single traits. In this French population, *A. thaliana* likely responded to both local warming and increased competition, in part mediated by central regulators of flowering time such as FLOWERING LOCUS C and TWIN SISTER OF FT. This genetic architecture, which includes both synergistic pleiotropic QTLs and distinct QTLs within particular micro-habitats, enables rapid phenotypic evolution while still maintaining genetic variation in wild populations.

Contemporary and rapid phenotypic evolution has been observed in many natural populations of plant and animal species[1,5], especially during invasion[6] and in response to both global climate change[7] and toxic pollution[8]. A handful of studies have identified the genetic architecture of contemporary adaptive evolution of qualitative traits (such as industrial melanism)[9] or single quantitative traits (such as herbicide detoxification in weeds or heavy-metal tolerance)[10,11]. However, the genetic architecture of many traits simultaneously experiencing contemporary adaptive evolution, especially assayed at the level of whole genomes, remains unexplored, despite its significance for predicting evolutionary trajectories of natural populations[12].

There are many factors that will impact the evolutionary trajectory of a natural population. In addition to well recognized factors such as the source of adaptive genetic variation[13,14] and the scenario of environmental change[14,15], theoretical studies predict that the number and effect sizes of alleles underlying multi-trait adaptive evolution depends on the magnitude of pleiotropy[3,4,16]. This relationship was first investigated using Fisher's geometric model, in which every mutation potentially affects all traits. Under this model, the rate of adaptation of an allele should decrease with its degree of pleiotropy[4] due to the increased probability of antagonistic effects of a mutation when more traits are impacted. In other words, the probability that a mutation is advantageous to one trait but detrimental to another trait increases with the degree of pleiotropy, leading to the concept of the so-called 'cost of complexity'[4]. However, in contrast to the assumptions of the geometric model, laboratory studies performed on yeast, nematode and mouse have found that the degree of pleiotropy follows an L-shaped distribution such that most mutations affect only a small subset of traits[3,16]. This distribution would diminish the 'cost of complexity'[3,4].

Of additional importance is the relationship between the degree of pleiotropy and the per-trait effect size of a mutation (termed pleiotropic scaling)[3,16]. Most theoretical models assume that the per-trait effect size of a mutation decreases (invariant total effect model) or remains constant (Euclidean superposition model) with the degree of pleiotropy[4]. Laboratory studies, on the other hand, have found synergistic pleiotropy in which the per-trait effect size of a mutation increases with the number of traits affected by that mutation[3]. Because this scaling property leads to an increased fitness advantage for more pleiotropic mutations, any cost of complexity is expected to be greatly alleviated[4]. Consequently, the combination of restricted and synergistic pleiotropy leads to the prediction that polymorphisms with intermediate degrees of pleiotropy, while rare, should have the highest rate of adaptive evolution[3,4]. This prediction is yet to be tested empirically.

In its most general sense, pleiotropy refers to the shared impact of SNPs. This can include the effect of a SNP on (i) multiple phenotypic traits in one environment, referred to as morphological pleiotropy[3], (ii) a single phenotypic trait among environments, referred to as environmental pleiotropy[3], or (iii) multiple traits in multiple environments, hereafter named morpho-environmental pleiotropy. Because wild populations evolve in complex abiotic and biotic environments, an exploration of the role of pleiotropy requires consideration of the impact of spatial environmental heterogeneity. In particular, when the same SNPs are favored in distinct micro-habitats, then the suite of selective effects may combine to drive rapid adaptive evolution whereas competing demands on a SNP across micro-sites might inhibit adaptive evolution.

In this study, we aimed to generate a comprehensive and unbiased view of how a local population of the annual model plant, *Arabidopsis thaliana,* changed over an eight year period in nature. During this time period, our natural population experienced climate change while it

evolved in an environment that is spatially heterogeneous in terms of both biotic and abiotic factors. Thus, this study adopts the modern standards of ecological genomics to describe the genetic architecture underlying rapid phenotypic evolution of multiple quantitative traits within a local plant population *in situ*.

RESULTS AND DISCUSSION

Our study focused on the local population TOU-A (East of France; **Supplementary Fig. 1**) that experienced an increase in mean annual temperature of more than 1°C over the last 30 years (**Supplementary Fig. 2**). The site occupancy by *A. thaliana* additionally increased between 2002 and 2007 and remained stable thereafter (**Supplementary Fig. 1**). Seeds of 80 and 115 individual plants (hereafter named accessions) were collected in 2002 and 2010, respectively. Previous studies conducted on accessions collected in 2002 showed that this population has an estimated outcrossing rate of 6%[17] and is highly diverse at both genetic (based on genotyping at 149 SNPs) and phenotypic levels[17-20]. In addition, the TOU-A population presents fine-scale spatial variation for a broad range of soil characteristics and is located between two permanent meadows dominated by grasses (**Supplementary Figs. 1 and 3**).

A resurrection experiment revealed rapid phenotypic evolution.

To identify phenotypic traits exhibiting evolutionary change within eight years, we established a resurrection experiment in which the 195 accessions collected in 2002 and 2010 were grown under common environmental conditions. This design enabled us to differentiate plastic from genetic responses[21]. The 195 accessions were grown *in situ* in six representative micro-habitats, consisting of three contrasting soil types crossed with the presence or absence of the bluegrass *Poa annua*, a species frequently associated with *A. thaliana*[20]

(**Supplementary Fig. 1**). A total of 5,850 plants were scored for 29 traits related to phenology, resource acquisition, shoot architecture, seed dispersal, fecundity, reproductive strategy and survival[22]. We detected significant genetic evolution for 16 out of the 29 traits (**Fig. 1a, Supplementary Table 1**). For example, we found a significant mean delay of 6.1 days for bolting time and a significant mean increase of ~7% in the number of fruits produced on the main stem (**Fig. 2a**). Interestingly, no evolutionary change was observed for average total seed production across the six micro-habitats, demonstrating that constant seed numbers can be maintained through evolution of flexible life-history and individual reproductive traits. A comparison of our results with the rates of evolution in other plant species[23] suggests a moderate rate of mean phenotypic evolution in the TOU-A population (**Fig. 2a**).

Analysis of our sequences of the genomes of the 195 accessions (~25x coverage) confirmed that the mean phenotypic change we observed was not the result of immigration from other phenotypically diverse populations. We observed extensive genetic variation, detecting 1,902,592 Single Nucleotide Polymorphisms, only 5.6 times less than observed in a panel of 1135 worldwide accessions[24]. However, the TOU-A population appears strongly genetically isolated from other local populations sampled within 1km (**Fig. 3a**), confirming the negligible role of immigration in the observed phenotypic change.

Similar phenotypic evolution associated with strong genotype-by-environment interactions.

We dissected the phenotypic evolution within each micro-habitat to test whether local abiotic and biotic growing conditions affect the genotype-phenotype relationships in the TOU-A population. Across the 29 traits measured in the six micro-habitats, 144 of these 174 eco-phenotypes displayed significant genetic variance (**Fig. 1b**), with broad-sense heritability estimates ranging from 0.20 to 0.87 (mean H^2 = 0.57, median H^2 = 0.60; **Supplementary**

142 **Table 2**). Average values of the phenotypes differed substantially among the six micro-
143 habitats (**Fig. 2b, Supplementary Table 1**). The proportions (ranging from 22.7% to 76.2%)
144 and identities of genetically variable traits that evolved in our eight-year timespan also
145 depended on the micro-habitat (**Figs. 1b and 2c**). These results highlight the need to consider
146 fine-scale environmental conditions to obtain an accurate picture of the diversity of micro-
147 evolutionary phenotypic processes occurring within a population.

148 Although each trait that evolved was consistent in its direction in all micro-habitats
149 (**Fig. 1b**), we observed highly significant changes in the ranking of accessions among micro-
150 habitats for most traits, with a mean across-micro-habitat genetic correlation of 0.46 (median
151 = 0.46, min = 0.04, max 0.89) (**Supplementary Table 1, Supplementary Fig. 4**). For
152 example, increased allocation of reproduction to the main stem was consistently observed but
153 different accessions most strongly manifested this allocation pattern among micro-habitats
154 (**Supplementary Fig. 5**). These results are in accordance with previous studies revealing
155 genotype-by-environment interactions for plant fitness-related traits at the scale of a few
156 meters[25,26]. However, the existence of genotype-by-environment interactions does not clarify
157 the extent of pleiotropy governing phenotypes in alternative micro-habitats: phenotypic
158 evolution toward the same optimum may be driven by loci harboring alleles differing in the
159 magnitude of allelic effects across micro-habitats and/or by distinct genetic bases in different
160 micro-habitats[27].

161 **Pleiotropy is restricted and synergistic**

162 To characterize the genetics underlying these environmentally dependent genotype-
163 phenotype relationships, we used GWA mapping to determine the genetic architecture, the
164 magnitude of pleiotropy and the extent of pleiotropic scaling. The TOU-A population is well-
165 suited for GWA mapping because it is phenotypically diverse and linkage disequilibrium
166 (LD) decays to $r^2 = 0.5$ within an average of 18 base pairs (**Fig. 3b**). In agreement with

limited LD, we observed an L-shaped distribution of the size of LD blocks, with a median size of 780bp (mean size = 5.5kb) (**Supplementary Fig. 6**). To verify our ability to finely map genomic regions associated with phenotypic variation, we first tested for the presence of significant associations of known functional polymorphisms. We successfully identified three known functional genes conferring either qualitative or quantitative resistance against bacterial pathogens when the 195 TOU-A accessions were infected under controlled conditions. In two of the three cases, the most highly associated SNP (hereafter named top SNP) was located within the gene (*RPS2* and *RKS1*)[19,28] and in the third case it was located 15 bp away (*RPM1*)[29] (**Supplementary Fig. 7**).

To further assess the efficacy of GWAS mapping in the TOU-A population, we followed the methodology used in Brachi *et al.* (2010)[30] to calculate enrichments for *a priori* candidate genes for bolting time in the six *in situ* micro-habitats (**Fig. 1b**). Because bolting time is a quantitative trait for which the genetic network has been extensively studied, it is well suited for calculating enrichments for *a priori* candidate genes. Similar to previous results for a field trial utilizing 197 worldwide accessions[30], the enrichment ratio quickly dropped with the number of top SNPs in five out of the six micro-habitats, demonstrating that candidate genes were overrepresented among top-ranking SNPs (**Fig. 4a, Supplementary Fig. 8**).

Here, we illustrate the impacts of genetic architecture, magnitude of pleiotropy and pleiotropic scaling when considering the 200 top SNPs (0.01% of the total number of SNPs) for each of the 144 eco-phenotypes that were heritable. Although we observed significant enrichment for up to the 500 SNPs, focus on only 200 top SNPs is conservative in defining pleiotropy and increases the fraction of true positives. Our choice of threshold does not matter: our biological conclusions are robust to successive cutoffs of top SNPs within the range of 50-500 SNPs, and to three successive cutoffs in terms of the significance of SNPs (-

192 $\log_{10}$ *p*-value > 6, -$\log_{10}$ *p*-value > 5, -$\log_{10}$ *p*-value > 4; chosen based on van Rooijen *et al.*
193 2015, Thoen *et al.* 2016, Kooke *et al.* 2017)[31,33].

194 We first compared the genetic architecture among micro-habitats for GWA results
195 from each of the 144 heritable eco-phenotypes (**Supplementary Fig. 9**). The number of genes
196 located within 2kb of the 200 top SNPs ranged from 45 (fruit number on basal branches in
197 soil B with *P. annua*) to 141 (maximum height scored in soil B without *P. annua*) (mean =
198 105 genes, median = 108 genes; **Supplementary Fig. 10**). For a given phenotypic trait, the
199 numbers of associated genes and their corresponding allelic effects sometimes varied widely
200 across micro-habitats, even when broad-sense heritabilities were similar (**Supplementary**
201 **Fig. 10, Supplementary Table 2**); for one dramatic example, see the results for bolting time
202 (**Fig. 4a, Supplementary Fig. 11**).

203 The extent of pleiotropy for each top SNP was determined by calculating an effective
204 number of eco-phenotypes, N_{eff}, sharing a given top SNP according to Pavlicev *et al.* (2009)[34].
205 This statistic corrects for correlations among eco-phenotypes to produce a measure of
206 pleiotropy that is not inflated. In agreement with previous laboratory observations on yeast,
207 nematode and mouse[3], we found that N_{eff} follows an L-shaped distribution (**Fig. 5a**). More
208 than 78% of top SNPs impacted a single trait in a single micro-habitat, indicating that genetic
209 bases are largely distinct across micro-habitats (**Supplementary Fig. 12 and 13**), as
210 illustrated for bolting time (**Fig. 4b**). As previously noted for yeast, nematode and mouse[3,16],
211 this pattern of restricted pleiotropy is more consistent with the notion of modular pleiotropy
212 (with genes being organized into structured networks) than universal pleiotropy in Fisher's
213 geometric model (i.e. each gene affects every trait)[3,4].

214 Pleiotropic SNPs were most frequently those demonstrating morpho-environmental
215 pleiotropy. In particular, the relative frequency of morpho-environmental pleiotropy increased

rapidly with the overall degree of pleiotropy, just as morphological pleiotropy became relatively less common (**Supplementary Fig. 14**). Perhaps surprisingly, there were very few examples of environmental pleiotropy, in which a significant SNP impacted the same trait in multiple environments. Our observation of the predominance of morpho-environmental pleiotropy is consistent with previous studies in *A. thaliana* reporting that the identity of traits affected by a gene can depend on the abiotic and biotic phenotyping environment[35-36] and highlights the importance of spatial environmental heterogeneity in determining the role of pleiotropy on phenotypic evolution of a suite of quantitative traits.

We found that the total effect size of a top SNP, calculated by either the Manhattan distance (T_M) or the Euclidean distance (T_E), increased with N_{eff} faster than linearly ($T_M = c^* {N_{eff}}^d$, d = 1.226 ± 0.003; $T_E = a^* Neff^b$, b = 0.724 ± 0.0035; **Fig. 5b, Supplementary Fig. 13 and 15, Supplementary Tables 3 and 4**). This empirical pattern of synergistic pleiotropy contrasts with most theoretical models, which typically assume that the per-trait effect size of a mutation decreases (d = 0.5 or b = 0, invariant total effect model) or remains constant (d = 1 or b = 0.5, Euclidean superposition model) with the degree of pleiotropy[4]. While previously observed in controlled laboratory conditions[3], our study reveals that such a pattern of synergistic pleiotropy can also extend to phenotypes scored in ecological realistic conditions. It should be noted that the non-linear relationship between total effect size and degree of pleiotropy is robust to successive decreasing cutoffs of N_{eff} (**Supplementary Table 5**), suggesting that the pattern of synergistic pleiotropy detected in our study is not driven solely by highly pleiotropic SNPs.

Intermediate degrees of synergistic pleiotropy drive adaptive evolution.

According to theoretical predictions[3,4], the combination of an L-shape distribution of N_{eff} and synergistic pleiotropy should lead polymorphisms with intermediate degrees of

pleiotropy, while rare, to experience the highest rates of adaptive evolution. One approach for determining rates of adaptive evolution is to measure the fitness impact of particular SNPs in particular environments. Unfortunately, the fitness proxies that we measured (e.g., total seed production and survival) were not genetically variable in some micro-habitats (**Fig. 1b**). This does not imply an absence of selection because we did not measure key germination and seedling survival traits. Therefore, we instead estimated signatures of selection on top SNPs by testing for the homogeneity of differentiation across SNP markers between our two temporal samples. Such a population genomics approach allows taking into account both the effect of selective processes at all life-stages and the effect of local demographic history between 2002 and 2010.

A genome-wide scan for selection based on temporal differentiation (F_{ST}) (**Supplementary Fig. 16**) revealed a signature of selection for top SNPs associated with evolved eco-phenotypes, but not for top SNPs associated with unevolved eco-phenotypes; top SNPs jointly associated with evolved and unevolved eco-phenotypes revealed an intermediate signature of selection (**Fig. 5c, Supplementary Fig. 13**). Because temporal differentiation was tested against changes in the genomic background, this result rejects the hypothesis of selectively neutral evolution for evolved eco-phenotypes. When focusing attention on top SNPs associated with evolved eco-phenotypes, we found that single-trait micro-habitat-specific SNPs were weakly differentiated while SNPs exhibiting an intermediate degree of pleiotropy revealed the largest fold-increase of median temporal F_{ST} values (**Fig. 5d, Supplementary Fig. 13**). This pattern is strengthened when considering only the top SNPs for evolved phenotypes that have a polarity of effects in line with the direction of phenotypic evolution (~75.4% of the total number of top SNPs associated with evolved eco-phenotypes; **Supplementary Fig. 17**). In addition, we found that the mean F_{ST} value of the top SNPs was significantly and positively associated with estimates of phenotypic evolution (i.e. *haldanes*)

when we considered the evolved eco-phenotypes, but not when we considered the unevolved eco-phenotypes (**Supplementary Fig. 18**). Taken together, and considering the prevalence of morph-environmental pleiotropy observed at intermediate degrees of pleiotropy (**Supplementary Fig. 14**), our results suggest the evolution of a common adaptive strategy that was accelerated due to top SNPs being shared across environments, although they affect different traits in different environments.

As previously highlighted for the patterns of restricted pleiotropy and synergistic pleiotropy, the relationships between degree of pleiotropy and signatures of selection were robust to different number of top SNPs and thresholds of significance (within the range considered; **Supplementary Fig. 13**).

Identity of candidate genes under directional selection.

The most pleiotropic genes underlying adaptive evolution in the TOU-A population were determined by retrieving all genes associated with 11 or more evolved eco-phenotypes. Among the 14 candidate genes (**Supplementary Table 6**), was the floral integrator *TWIN SISTER OF FT* (*TSF*), which was associated with bolting time (three microhabitats), flowering interval (one micro-habitat), the length of reproductive period (three micro-habitats), the number of primary branches (one micro-habitat) and the escape strategy to competition (three micro-habitats). Interestingly, based on a panel of 948 worldwide accessions of *A. thaliana*, *TSF* has been found to be significantly associated with climate variation (i.e. number of consecutive cold days)[37], suggesting that *TSF* may play a major role in the adaptation of *A. thaliana* to climate at different geographical scales.

We additionally tested for biological processes that were enriched in the extreme tail of our genome-wide temporal differentiation scan (**Supplementary Table 7**). In total, 24 biological processes were enriched, 15 of which were supported by genes associated with

289 phenotypic traits measured in this study (**Supplementary Table 7**). Enrichment for
290 vernalization response was supported by *VERNALIZATION2* (*VRN2*) associated with six eco-
291 phenotypes including two proxies of fitness (i.e. survival and seed production,
292 **Supplementary Table 7**). We also detected many related, enriched functions such as stamen
293 development, pollen maturation and callose deposition (**Supplementary Table 7**), which are
294 consistent with the simultaneous evolution of fecundity traits observed in this study (**Fig. 1**).
295 For instance, the candidate gene *POWDERY MILDEW RESISTANT 4* is traditionally regarded
296 as a defense response to wounding and pathogens due to its role in reinforcing the cell wall,
297 although it is also essential for pollen viability and cell division[38]. In this study, *POWDERY*
298 *MILDEW RESISTANT 4* was associated with two fecundity traits: mean fruit length on
299 primary branches (in soil A without *P. annua*) and the number of fruits on the main stem (in
300 soil C with *P. annua*; **Supplementary Table 7**). The simultaneous evolution of fecundity
301 traits suggests an adaptive strategy of short-lived semelparous species like *A. thaliana* in
302 crowded environments, where plants tend to escape competition[20,39]. In agreement with this
303 hypothesis, we observed an evolution of the escape strategy trait in five out of six micro-
304 habitats (**Fig. 1b**).

305 The remaining nine enriched biological processes were supported by genes that were
306 not associated with any measured phenotype. This is not surprising in that we missed the
307 entire seed and seedling stage, and did not capture the entire suite of biotic and abiotic factors
308 that can impact selection over time. Among these candidate genes was the MADS-box
309 transcription factor *FLOWERING LOCUS C* (*FLC*) that, in agreement with the recent local
310 warming experienced by the TOU-A population, supported the strong enrichment detected for
311 vernalization response, response to temperature stimulus and regulation of circadian rhythm
312 (**Supplementary Table 6**). *FLC* is a well-known pleiotropic gene[40] that affects many traits
313 that we did not measure (such as vernalization response, water use efficiency and regulation

of seed dormancy by maternal temperature)[41-44], suggesting that one or more of these traits may have undergone contemporary and rapid phenotypic evolution in the TOU-A population. For example, the proportion of accessions with a slow rather than rapid vernalization haplotype at *FLC*[42] increased between 2002 and 2010 (Chi-squared test = 16.554, P = 0.000047; **Supplementary Fig. 19**). Such a pattern is understandable in light of the increase in the number of chilling degree days observed between 2002 and 2010 (**Supplementary Fig. 2).**

It is interesting to note that we identified two central regulators of flowering time in our set of candidate pleiotropic genes, *i.e. FLC* and *TSF*. In two *Brassica rapa* populations that evolved rapidly following drought in Southern California[12], rapid evolution was in part mediated by a homologue of *SUPPRESSOR OF OVEREXPRESSION OF CONSTANS 1* (*SOC1*), a target of *FLC*-mediated transcriptional repression[45], suggesting that central regulators of flowering time play a major role in the response to global warming.

CONCLUSION

Our ecological genomic comparison of plants separated by eight generations revealed rapid multi-trait adaptive evolution that was similar among six micro-habitats, but largely mediated by different genes. The strong genotype-by-environment interactions highlight the importance of considering fine-scale ecological variation. By limiting the erosion of standing genetic variation, this micro-habitat dependent genetic architecture should allow populations like TOU-A to continue to respond to future environmental changes.

In addition, the combination of GWAS and an *in situ* resurrection experiment validated the prediction that polymorphisms with intermediate degrees of pleiotropy, while rare, should have the highest rate of adaptive evolution. This result reinforces the importance

of simultaneous evolution of multiple traits in shaping the genomic adaptive trajectory of natural populations. On-going resurrection projects in plants[46] and long-term population surveys of wild animals[47] represent an exciting opportunity to test whether restricted pleiotropy combined with synergistic pleiotropy also underlies contemporary and rapid adaptive evolution in other plant and animal species.

ACKNOWLEDGEMENTS

We are grateful to Benjamin Brachi for his helpful discussions on the enrichment analysis in biological processes. This work was funded by the Région Midi-Pyrénées (CLIMARES project), the INRA Santé des Plantes et Environnement department (RESURRECTION project), the INRA-ACCAF metaprogram (SELFADAPT project), the LABEX TULIP (ANR-10-LABX-41, ANR-11-IDEX-0002-02) and the National Institute of Health.

AUTHOR CONTRIBUTIONS

F.R. supervised the project. F.R. conceived of and designed the experiments. E.B., L.A., Ro.V and F.R. conducted the *in situ* experiment. L.F., C.G., C.H.C. and F.R. measured the phenotypic traits. L.F. and F.R. analyzed the phenotypic traits. O.B. and M.V. generated the sequencing data. S.B. and C.L. performed the bioinformatics analyses. L.F., C.L. and F.R. performed the GWA mapping. L.F., C.L., D.R. and F.R. performed and analyzed the enrichment tests. M.N., L.G. and Re.V. developed a methodology in selfing species to perform a genome-wide scan for selection based on temporal differentiation. V.L.C and J.B guided the analysis of phenotypic and genomic data. F.R. and J.B. wrote the manuscript, with contributions from L.F., C.L, Ro.V., M.N., L.G., Re.V. and D.R. All authors contributed to the revisions.

REFERENCES

1. Franks, S.J., Weber, J.J. & Aitken, S.N. Evolutionary and plastic responses to climate changes in terrestrial plant populations. *Evol. Appl.* 7, 123-139 (2014).
2. Bay, A.B., Rose, N., Barrett, R., Bernatchez, L., Ghalambor, C.K., Lasky, J.R., Brem, R.B., Palumbi, S.R. & Ralph, P. Predicting responses to contemporary environmental change using evolutionary response architectures. *Am. Nat.* **189** (2017).
3. Wang, Z., Liao, B.-Y. & Zhang, J. Genomic patterns of pleiotropy and the evolution of complexity. *Proc. Natl. Acad. Sci. U.S.A.* **107**, 18034-18039 (2010).
4. Wagner, G.P. & Zhang, J. The pleiotropic structure of the genotype – phenotype map: the evolvability of complex organisms. *Nat. Rev. Genet.* **12,** 204-213 (2011).
5. DeLong, J.P., Forbes, V.E., Galic, N., Gibert, J.P., Laport, R.G., Phillips, J.S. & Vavra J.M. How fast is fast? Eco-evolutionary dynamics and rates of change in populations and phenotypes. *Ecol. Evol.* **6,** 573-581 (2016).
6. Buswell, J.M., Moles, A.T. & Hartley, S. Is rapid evolution common in introduced plant species? *J. Ecol.* **99,** 214-224 (2011).
7. Franks, S.J., Sim, S. & Weis, A.E. Rapid evolution of flowering time by an annual plant in response to a climate fluctuation. *Proc. Natl. Acad. Sci. U.S.A.* **104**: 1278-1282 (2007).
8. Reid, N.M., Proestou, D.A., Clark, B.W., Warren, W.C., Colbourne, J.K., Shaw, J.R., Karchner, S.I., Hahn, M.E., Nacci, D., Oleksiak, M.F., Crawford, D.L. & Whitehead, A. The genomic landscape of rapid repeated evolutionary adaptation to toxic pollution in wild fish. *Science* **354,** 1305-1308.

9. van't Hof, A.E., Edmonds, N., Dalikova, M., Marec, F. & Saccheri, I.J. Industrial melanism in British peppered moths has a singular and recent mutational origin. *Science* **332,** 958-960.
10. Hanikenne, M., Talke, I.N., Haydon, M.J., Lanz, C., Nolte, A., Motte, P., Kroymann, J., Weigel, D. & Krämer, U. Evolution of metal hyperaccumulation required *cis*-regulatory changes and triplication of *HMA4*. *Nature* **453,** 391-395.
11. Délye, C., Jasieniuk, M. & Le Corre V. Deciphering the evolution of herbicide resistance in weeds. *Trends Genet.* **29,** 649-658.
12. Franks, S.J., Kane, N.C., O'Hara, N.B., Tittes, S. & Rest, J.S. Rapid genome-wide evolution in *Brassica rapa* populations following drought revealed by sequencing of ancestral and descendant gene pools. *Mol. Ecol.* **25,** 3622-3631 (2016).
13. Dittmar, E.L., Oakley, C.G., Conner, J.K., Gould, B.A. & Schmeske, D.W. Factors influencing the effect size distribution of adaptive substitutions. *Proc. Roy. Soc. B.* **283,** 20153065 (2016).
14. Matuszewski, S., Hermisson, J. & Kopp, M. Catch me if you can: adaptation from standing genetic variation to a moving phenotypic optimum. *Genetics* **200,** 1255-1274 (2015).
15. Kopp, M. & Matuszewski, S. Rapid evolution of quantitative traits: theoretical perspectives. *Evol. Appl.* **7,** 169-191 (2014).
16. Wagner, G.P. *et al.* Pleiotropic scaling of gene effects and the 'cost of complexity'. *Nature* **452,** 470-472 (2008).
17. Platt, A. *et al.* The scale of population structure in *Arabidopsis thaliana*. *PLoS Genet.* **6**, e1000843 (2010).
18. Brachi, B. *et al.* Investigation of the geographical scale of adaptive phenological variation and its underlying genetics in *Arabidopsis thaliana*. *Mol. Ecol.* **22**, 4222-4240 (2013).

19. Huard-Chauveau, C. *et al.* An atypical kinase under balancing selection confers broad-spectrum disease resistance in Arabidopsis. *PLoS Genet.* **9**, e1003766 (2013).
20. Baron, E., Richirt, J., Villoutreix, R., Amsellem, L. & Roux, F. The genetics of intra- and interspecific competitive response and effect in a local population of an annual plant species. *Funct. Ecol.* **29**, 1361-1370 (2015).
21. Franks, S.J. *et al.* The resurrection initiative: storing ancestral genotypes to capture evolution in action. *BioScience* **58**, 870-873 (2008).
22. Roux, F., Mary-Huard, T., Barillot, E., Wenes, E., Botran, L., Durand, S., Villoutreix, R., Martin-Magniette, M.-L., Camilleri, C. & Budar, F. Cytonuclear interactions affect adaptive phenotypic traits of the annual plant *Arabidopsis thaliana* in ecologically realistic conditions. *Proc. Natl. Acad. Sci. U.S.A.* **113**: 3687-3692 (2016).
23. Bone, E. & Farres, A. Trends and rates of microevolution in plants. *Genetica* **112-113**, 165-182 (2001).
24. The 1001 Genomes Consortium. 1,135 genomes reveal the global pattern of polymorphism in *Arabidopsis thaliana*. *Cell* **166**, 1-11 (2016).
25. Kalisz, S. Variable selection on the timing of germination in *Collinsia verna* (Scrophulariaceae). *Evolution* **40,** 479-491 (1986).
26. Stratton, D.A. Spatial scale of variation in fitness of *Erigeron annuus*. *Am. Nat.* **146,** 608-324 (1995).
27. Des Marais, D.L., Hernandez, K.M. & Juenger, T.E. Interaction and plasticity : exploring genomic responses of plant to the abiotic environment. *Annu. Rev. Ecol. Evol. Syst.* **44**, 5-29 (2013).
28. Bent, A.F., Kunkel, B.N., Dahlbeck, D., brown, K.L., Schmidt, R., Giraudat, J., Leung, J. & Staskawicz, B.J. *RPS2* of *Arabidopsis thaliana*: a leucine-rich repeat class of plant disease resistance genes. *Science* **265,** 1856-1860 (1994).

29. Grant, M.R., Godirad, L., Straube, E., Ashfield, T., Lewald, J., Sattler, A., Innes, R.W & Dangl J.L. Structure of the Arabidopsis *RPM1* gene enabling dual specificity disease resistance. *Science* **269,** 843-846 (1995).

30. Brachi, B. *et al.* Linkage and association mapping of *Arabidopsis thaliana* flowering time in nature. *PLoS Genet.* **6:**e1000940 (2010).

31. Van Rooijen, R., Aarts, M.G.M. & Harbinson, J. Natural genetic variation for acclimation of photosynthetic light use efficiency to growth irradiance in Arabidopsis. *Plant Physiol.* **167,** 1412-1429 (2015).

32. Kooke, R., Kruijer, W., Bours, R., Becker, F., Kuhn, A., van de Geest, H., Buntjer, J., Doeswijk, T., Guerra, J., Bouwmeester, H., Vreugdenhil, D. & Keurentjes, J.B. Genome-wide association mapping and genomic prediction elucidate the genetic architecture of morphological traits in Arabidopsis. *Plant Physiol.* **170,** 2187-2203 (2016).

33. Thoen, M.P.M. *et al.* Genetic architecture of plant stress resistance: multi-trait genome-wide association mapping. *New Phytol.* **213,** 1346-1362 (2016).

34. Pavlicev, M., Cheverud, J.M. & Wagner, G.P. Measuring morphological integration using eigenvalues variance. *Evol. Biol.* **36,** 157-170 (2009).

35. Korves, T. & Bergelson, J. A novel cost of *R* gene resistance in the presence of disease. *Am. Nat.* **163,** 489-504 (2004).

36. Scarcelli, N., Cheverud, J.M., Schall, B.A. & Kover, P.X. Antagonistic pleiotropic effect reduce the potential adaptive value of the FRIGIDA locus. *Proc. Natl. Acad. Sci. U.S.A.* **104,** 16986-16991 (2007).

37. Hancock, A.M. *et al.* Adaptation to climate across the *Arabidopsis thaliana* genome. Science **334**, 83-86 (2011).

458 38. Ellinger, D. & Voigt, C.A. Callose biosynthesis in Arabidopsis with a focus on pathogen
459 response: what we have learned with the last decade. *Annals of Botany* **114**, 1349-1358
460 (2014).
461 39. Bonser, S.P. High reproduction efficiency as an adaptive strategy in competitive
462 environments. *Funct. Ecol.* **27**, 876-885 (2013).
463 40. Deng, W. *et al. FLOWERING LOCUS C* (*FLC*) regulates development pathways
464 throughout the life cycle of *Arabidopsis*. *Proc. Natl. Acad. Sci. U.S.A.* **108**, 6680-6685
465 (2011).
466 41. McKay, J.K., Richards, H. & T. Mitchell-Olds. Genetics of drought adaptation in
467 *Arabidopsis thaliana*: I. Pleiotropy contributes to genetic correlations among ecological
468 traits. *Mol. Ecol.* **12,** 1137-1151 (2013).
469 42. Li, P., Filiault, D., Box, M.S., Kerdaffrec, E., van Oosterhout, C., Wilczek, A.M.,
470 Schmitt, J., McMullan, M., Bergelson, J., Nordborg, M. & Dean, C. Multiple *FLC*
471 haplotypes defined by independent *cis*-regulatory variation underpin life history diversity
472 in *Arabidopsis thaliana*. *Genes Dev.* **28,** 1635-1640 (2014).
473 43. Blair, L., Auge, G. & Donohue, K. Effect of *FLOWERING LOCUS C* on seed
474 germination depends on dormancy. *Funct. Plant Biol.* **44,** 493-506 (2017).
475 44. Auge, G., Blair, L.K., Neville, H. & Donohue, K. Maternal vernalization and
476 vernalization-pathway genes influence seed germination. *New Phytol.* doi:
477 10.1111/nph.14520 (2017).
478 45. Salathia, N. *et al. FLOWERING LOCUS C* - dependent and – independent regulation of
479 the circadian clock by the autonomous and vernalization pathways. *BMC Plant Biol.* **6,**
480 10 (2006).
481 46. Etterson, J.R. *et al.* Project Basline : an unprecedented resoruce to study plant evolution
482 across space and time. *Am. J. Bot.* **103,** 164-173 (2016).

47. Kruuk, L.E.B., Garant, D. & Charmantier, A. The study of quantitative genetics in wild populations. Pages 1-15 *In Quantitative genetics in wild populations*. Edited by A. Charmantier, D. Garant and L.E.B. Kruuk. Oxford University Press, Oxford, U.K. pp 1-15 (2014).

METHODS

Plant material. The population TOU-A is located under a 350m electric fence separating two permanent meadows experiencing cycles of periodic grazing by cattle in the village of Toulon-sur-Arroux (France, Burgundy, N 46°38'57.302'', E 4°7'16.892''). Seeds from individual plants were collected in 2002 (TOU-A-2002, n = 80) and 2010 (TOU-A-2010, n = 115) according to a sampling scheme allowing us to take into account the density of *A. thaliana* plants along a 350m transect (**Supplementary Fig. 1**). Differences in maternal effects among the 195 accessions collected in 2002 and 2010 were reduced by growing one plant per family under controlled greenhouse conditions, for one generation (16-h photoperiod, 20°C).

Ecological characterization. Eighty-three soil samples collected along the 350m transect were characterized for 14 edaphic factors[18]: pH, maximal water holding capacity (WHC), total nitrogen content (N), organic carbon content (C), C/N ratio, soil organic matter content (SOM), concentrations of P_2O_5, K, Ca, Mg, Mn, Al, Na and Fe. Climate data was generated with the ClimateEU v4.63 software package[48].

Phenotypic characterization. An experiment of 5,850 plants was set up at the local site of the TOU-A population. The 195 accessions collected in 2002 and 2010 were grown in six representative 'soil x competition' micro-habitats. Each of these micro-habitats was organized in five blocks. Each of the five blocks corresponded to an independent randomization of 195

plants with one replicate per accession collected in 2002 and 2010. Seeds were sown in late September to mimic the main natural germination cohort observed in the TOU-A population (**Supplementary Fig. 1**). Each plant was scored for a total of 29 phenotypic traits chosen to characterize the life history of *A. thaliana* including the timing of offspring production or seed dispersal, or because they are involved in the response to competition and/or are good estimators of life-time fitness and reproductive strategies[22].

Phenotypic analyses, natural variation, phenotypic evolution and evolutionary rates. We explored natural variation of all phenotypic traits using the following statistical mixed model:

$$Y_{ijklm} = \mu_{trait} + block_i\,(soil_j * comp_k) + soil_j + comp_k + soil_j * comp_k + year_l + soil_j * year_l + comp_k * year_l + soil_j * comp_k * year_l + accession_m\,(year_l)) + accession_m\,(year_l)) * soil_j + accession_m\,(year_l)) * comp_k + accession_m\,(year_l)) * soil_j * comp_k + \varepsilon_{ijklm} \qquad (1)$$

In this model, '*Y*' is one of the 29 phenotypic traits, 'μ' is the overall phenotypic mean; 'block' accounts for differences between the five experimental blocks within each type of 'soil * absence/presence of *P. annua*' experimental combination; 'soil' corresponds to the effects of the three types of soil; 'comp' measure the effect of the presence of *P. annua*; 'year' corresponds to effect of the two sampling years 2002 and 2010; 'accession' measures the effect of accessions within year; interaction terms involving the 'accession' term account for genetic variation in reaction norms of accessions between the three types of soil and the absence or presence of *P. annua*; and 'ε' is the residual term.

All factors were treated as fixed effects, except 'accession' that was treated as a random effect. For fixed effects, terms were tested over their appropriate denominators for calculating *F*-values. Significance of the random effects was determined by likelihood ratio tests of model with and without these effects. When necessary, raw data were either log

transformed or Box-Cox transformed to satisfy the normality and equal variance assumptions of linear regression. A correction for the number of tests was performed for each modeled effect to control the False Discovery Rate (FDR) at a nominal level of 5%.

Inference was performed using ReML estimation, using the PROC MIXED procedure in SAS 9.3 (SAS Institute Inc., Cary, North Carolina, USA) for all traits with the exception of SURVIVAL, which was analyzed using the PROC GLIMMIX procedure in SAS 9.3.

For all traits, Best Linear Unbiased Predictions (BLUPs) were obtained for each accession in each of the six experimental conditions, using the PROC MIXED procedure in SAS 9.3 (SAS Institute Inc., Cary, North Carolina, USA):

$$Y_{imc} = \mu_{\text{trait}} + \text{block}_i + \text{accession}_m + \varepsilon_{im} \quad (2)$$

For each trait, significant genetic variation among the accessions was detected by testing the significance of the 'accession' term in equation (2). A correction for the number of tests was performed for the modeled 'accession' effect (across the 29 traits within each of the six experimental conditions) to control the FDR at a nominal level of 5%. Because *A. thaliana* is a highly selfing species[13], BLUPs correspond to the genotypic values of accessions.

In each of the six experimental conditions, rates of evolutionary change based on genotypic values of accessions were calculated in *haldanes* (h_g) for all eco-phenotypes with significant genetic variation among the 195 accessions collected in 2002 and 2010. *haldanes* is a metric that scales the magnitude of change by incorporating trait standard deviations[49,50]. h_g values were calculated between 2002 and 2010, as:

$$h_g = \frac{(x_2/s_p) - (x_1/s_p)}{g} \quad (3)$$

where 'x' corresponds to the mean genotypic value at year 1 (TOU-A population collected in 2002) and year 2 (TOU-A population collected in 2010), 's_p' is the standard deviation of the genotypic values of the trait pooled across the two years, and 'g' is the number of generations. Because only one germination cohort was observed every year between 2002 and 2010 (i.e. fall germination cohort), only one generation per year was considered in the calculation of *haldanes* values. For a given trait, 95% confidence intervals were estimated based on the distribution of 1000 *haldanes* values obtained by bootstrapping 1000 random samplings with replacement of genetic values within each year. A *haldanes* value was considered significantly different from zero if its 95% confidence intervals did not overlap zero.

Sequencing and polymorphism detection. DNA-seq experiments were performed on an Illumina HiSeq2500 using a paired-end read length of 2x100 pb with the Illumina TruSeq SBS v3 Reagent Kits. Raw reads of each of the 195 accessions were mapped onto the TAIR10 *A. thaliana* reference genome Col-0 with a maximum of 5 mismatches on at least 80 nucleotides. A semi-stringent SNPCalling across the genome was then performed for each accession with SAMtools mpileup (v0.01019)[51] and VarScan (v2.3)[52] with the parameters corresponding to a theoretical sequencing coverage of 30X and the search for homozygous sites.

Patterns of linkage disequilibrium and geographic structure. Considering only SNPs with a Minor Allele Relative Frequency (MARF) > 0.07, the LD extent within 30kb-windows on each chromosome were estimated using *VCFtools*[53]. LD blocks across the genome were identified in the PLINK environment using the following parameters --blocks no-pheno-req --maf 0.07 --blocks-max-kb 200, leading to the identification of 19,607 blocks with at least two SNPs (mean number of SNPs per block = 47.6, median number of SNPs per block = 12, mean block length = 5.5kb, median block length = 0.78kb). To position the TOU-A population

582 within the French geographic structure, we retrieved the positions of the 214,051 SNPs
583 genotyped on 24 accessions within 10 populations located within 1km of the TOU-A
584 population[54] across the genomes of the TOU-A population. Clustering genotype analysis was
585 performed using the packages gdsfmt and SNPRelate in the *R* environment[55], using the
586 snpgdspLD pruning command with the following parameters *ld.threshold=0.8*
587 *slide.max.bp=500 maf=0.07*, leaving us with 90,883 SNPs.

588 **Genome-Wide Association mapping and MARF threshold.** GWA mapping was run using
589 a mixed-model approach implemented in the software EMMAX (Efficient Mixed-Model
590 Association eXpedited)[56]. This model includes a genetic kinship matrix as a covariate to
591 control for population structure.

592 Because of bias due to rare alleles[30,56,57], we estimated a MARF threshold above which
593 the *p*-value distribution is not dependent on the MARF. We plotted the 99% quantile of the *p*-
594 value distribution of all 144 eco-phenotypes (i.e. 'micro-habitat x trait' combinations)
595 displaying significant genetic variance (**Fig. 1**) along 50 MARF values (with an increment of
596 0.01 from 0.01 to 0.5). A locally-weighted polynomial regression indicated that *p*-value
597 distributions were dependent on MARF value. From visual inspection, we considered a
598 threshold of MARF value > 0.07, which resulted in a total number of 981,617 SNPs for the
599 following analyses (**Supplementary Fig. 20**).

600 **Enrichment for *a priori* candidate genes.** To determine the threshold number of top SNPs
601 (i.e. SNPs with the highest associations) above which additional top SNPs would behave like
602 the rest of the genome, we calculated enrichments for *a priori* candidate genes for natural
603 genetic variation of bolting time observed in the six *in situ* experimental conditions (**Fig. 1**).
604 Based on an algorithm described in Brachi *et al.*(2010)[30] and a list of 328 candidate genes for
605 bolting time[14], enrichment was calculated for progressively fewer selective sets of top SNPs

606 within a 20Kb window of an *a priori* candidate gene. For each set of top SNPs, a null
607 distribution of enrichment was computed to determine a 95% confidence interval[30].

608 **Degree of pleiotropy and pleiotropic scaling.** Each trait displaying significant genetic
609 variance in a given *in situ* micro-habitat was considered an "eco-phenotype". The degree of
610 pleiotropy of a given top SNP was defined as the number of eco-phenotypes that shared this
611 top SNP. To account for the correlations between eco-phenotypes that can overestimate the
612 degree of pleiotropy, we followed Wagner *et al.* (2008)[16] by estimating for each top SNP an
613 effective number of eco-phenotypes as $N_{\text{eff}} = N - \text{var}(\lambda)$ where $\text{var}(\lambda)$ is the variance of the
614 eigenvalues of the error-corrected matrix.

615 The allelic effects were calculated using the mixed model implemented in the software
616 EMMAX after fitting the pairwise genetic kinship effect[56]. Because different units were used
617 to measure the 29 traits scored in this study, we calculated a standardized allelic effect for
618 each eco-phenotype affected by a top SNP according to Wagner *et al.* (2008)[16]. The
619 standardized effect on eco-phenotype *i*, denoted by A_i, is half the difference in genotypic
620 means between the two homozygous genotypes. The total size of the phenotypic effects of a
621 top SNP was then calculated by the Manhattan distance[58] $T_{\text{M}} = \sum_{i=1}^{n} |A_i|$, where n is the
622 degree of pleiotropy and A_i is the standardized allelic effect[3,4,16]. The pleiotropic scaling
623 relationship between the total effect size and the effective number of eco-phenotypes was
624 calculated as $T_{\text{M}} = c^* {N_{\text{eff}}}^d$.

625 The pleiotropic scaling relationship between the total effect size and the effective
626 number of eco-phenotypes was also calculated as $T_{\text{E}} = a^* Neff^b$, with T_{E} corresponding to
627 the Euclidean distance and calculated as $T_{\text{E}} = \sqrt{\sum_{\text{i=1}}^{\text{n}} A_{\text{i}}^2}$, where n is the degree of pleiotropy
628 and A_i is the standardized allelic effect.

629 The degree of pleiotropy and the pleiotropic scaling relationship were calculated for (i)
630 five threshold number of top SNPs (i.e. 50 SNPs, 100 SNPs, 200 SNPs, 300 SNPs and 500

SNPs) and (ii) three thresholds of significance ($-\log_{10} p$-value > 6, $-\log_{10} p$-value > 5, $-\log_{10} p$-value > 4). To avoid pseudo-replication due to the presence of several top SNPs in a given LD block (n = 19,607 blocks with at least two SNPs), the pleiotropic scaling was also calculated for each threshold number of top SNPs and each threshold of significance, (i) by considering the mean value of T_M (or T_E) and N_{eff} per LD block containing top SNPs and (ii) by randomly sampling one top SNP per LD block (this step was repeated 1,000 times).

Genome-wide scan for selection based on temporal differentiation. In the following, we outline a procedure inspired by Goldringer & Bataillon (2004)[59] to test for the homogeneity of differentiation across SNP markers between two temporal samples. If all SNP markers are selectively neutral, they should provide estimates of temporal differentiation drawn from the same distribution, which depends on the strength of genetic drift in the population (and therefore on its effective size). In contrast, if some marker loci are targeted by selection (or if they are in linkage disequilibrium with selected variants), then some heterogeneity in locus-specific measures of temporal differentiation should be observed. This is due to selection that will tend to drive measures of differentiation to values greater (or smaller) than expected under drift alone. The rationale of our approach is therefore to identify those SNPs that show outstanding differentiation, compared to neutral expectation.

We measure temporal differentiation between sample pairs using F_{ST}. Although the F_C statistic[60] was used in Goldringer & Bataillon (2004)[59], estimators of F_{ST} have better statistical properties in terms of bias and variance, and multilocus estimates have been precisely defined and thoroughly evaluated[61].

Using a multilocus estimate of F_{ST} from the pair of temporal samples, we infer the

effective size of the population. Because the 195 *A. thaliana* accessions are considered highly homozygous across the genome, heterozygous sites were discarded (see above) and the data therefore consist of haploid genotypes. We considered a single haploid population of constant size N_e, which has been sampled at generation 0, and τ generations later. Generations do not overlap. New mutations arise at a rate μ, and follow the infinite allele model (IAM). Following Skoglund *et al.* (2014)[62], the pairwise parameter F_{ST} between the two samples can be read:

$$F_{ST} = \frac{1 - e^{-\theta T/2}}{1 + \theta - e^{-\theta T/2}}$$

where $T \equiv \tau / N_e$ and $\theta \equiv 2N_e\mu$. In the low mutation limit (i.e., as $\mu \to 0$):

$$F_{ST} \approx \frac{T}{T+2} = \frac{\tau}{\tau + 4N_e}$$

This suggests that a simple moment-based estimator of effective population size can be derived as:

$$\hat{N}_e = \frac{\tau(1 - \hat{\bar{F}}_{ST})}{4\hat{\bar{F}}_{ST}}$$

where $\hat{\bar{F}}_{ST}$ is a multilocus estimate of the parameter F_{ST}. In what follows, we use the estimator of Weir & Cockerham (1984)[61]; preliminary analyses showed that these estimates of effective size have lower bias and variance than averaged estimates based on single-locus estimates of F_C.

In this study, the pairwise differentiation between the 195 *A. thaliana* accessions samples collected in 2002 and 2010 based on the full set of 1,902,592 SNP markers was: $\hat{\bar{F}}_{ST}$ = 0.0215, which gives an estimate of $\hat{N}_e$ = 182 (measured as a number of gene copies).

For each SNP, we tested the null hypothesis that the locus-specific differentiation measured at this focal marker was only due to genetic drift. For this purpose, we computed the expected distribution of F_{ST} for each SNP, conditional upon the estimated effective size

677 (using the same estimated value for all markers: $\hat{N}_e$ = 182), and the allele frequencies at the
678 focal SNP in the initial sample (i.e. 80 accessions collected in 2002). We simulated individual
679 gene frequency trajectories, as follows:

680 Suppose that we observe k_0 copies of the reference allele, out of n_0 sampled genes, in
681 the 2002 sample. We assume that these observed counts are drawn from a binomial
682 distribution $B(n_0,\pi_0)$ where π_0 is the (unknown) allele frequency of the reference allele in the
683 population. Assuming a Beta(1,1) prior distribution for π_0 (uniform distribution), and using
684 the Bayes inversion formula, the posterior distribution of π_0 is a Beta(k_0 + 1,$n_0 - k_0$ + 1). For
685 each marker and for each simulation, we therefore draw the initial allele frequency $\tilde{\pi}_0$ from a
686 Beta(k_0 + 1,$n_0 - k_0$ + 1). We then draw "pseudo-observed" allele counts using a random draw
687 from $B(n_0, \tilde{\pi}_0)$. This procedure allows accounting for the sampling variance in initial allele
688 frequencies, instead of fixing $\tilde{\pi}_0$ to the observed frequency in the sample, as previously done
689 in Goldringer & Bataillon (2004)[59].

690 Then, we simulated eight generations of drift, using successive binomial draws with
691 parameters $\hat{N}_e$ = 182 and the allele frequency in the previous generation. In the last
692 generation, a sample of genes is taken as a binomial draw with parameters n_τ (the sample size
693 in 2010), and $\tilde{\pi}_\tau$ (the simulated allele frequency in the last generation).

694 Last, we computed locus-specific estimates of temporal F_{ST} from the simulated allele
695 counts at the initial and last generation. The whole procedure was repeated at least 10,000
696 times for each marker (additional simulations were performed for some markers to obtain
697 non-null *p*-values).

698 Finally, we assigned a *p*-value to each SNP marker, computed as the proportion of
699 simulations giving a locus-specific estimate of F_{ST} larger than or equal to the observed value
700 at the focal SNP. We checked that the distribution of *p*-values was fairly uniform (data not

shown).

Note that all SNP markers with a MARF ≤ 0.07 (computed as the overall frequency across the two temporal samples) were discarded from the analysis. There were 981,617 remaining loci (**Supplementary Fig. 7**). To avoid any potential bias, all the distributions of F_{ST} were obtained using only simulated markers with a MARF > 0.07.

Enrichment analysis of top SNPs for signals of selection. Based on the effective number of eco-phenotypes affected by a SNP, we tested whether top SNPs related to evolved eco-phenotypes rejected the hypothesis of selectively neutral evolution more often than top SNPs related to unevolved eco-phenotypes for any given degree of pleiotropy. For each set of top SNPs (i.e. top SNPs that hit only evolved eco-phenotypes, top SNPs that hit only unevolved eco-phenotypes and top SNPs that hit both types of eco-phenotypes), we first computed a fold-increase in median significance of F_{ST} values using the following ratio: $ratio_{significance}$ = median of $-\log_{10}(p\text{-values})$ of F_{ST} values of n top SNPs / median of $-\log_{10}(p\text{-values})$ of F_{ST} values of n SNPs randomly sampled across the genome, where n = number of top SNPs. This step was repeated 1,000 times, generating a distribution of fold-increase in median significance of F_{ST} values of top SNPs. We assigned a p-value by computing the proportion of $ratio_{significance}$ smaller or equal to 1. The random sampling was done according to a scheme that results in sets of SNPs that resemble the original set with respect to linkage disequilibrium[37].

We then tested whether the strength of selection differed among the degrees of pleiotropy by computing a fold-increase in median F_{ST} values for each set of top SNPs, using the following ratio: $ratio_{values}$ = median of F_{ST} values of n top SNPs / median of F_{ST} values of all SNPs. This step was repeated 1,000 times, by randomly sampling the same number n of SNPs across the genome. This procedure generated a null distribution of fold-increase in median F_{ST} values. We assigned a p-value by comparing $ratio_{values}$ calculated for the set of top SNPs to the quantiles at 95%, 99% and 99.9% of the null distribution.

726 The enrichment analysis of top SNPs for signals of selection was calculated for (i) five
727 threshold number of top SNPs (i.e. 50 SNPs, 100 SNPs, 200 SNPs, 300 SNPs and 500 SNPs)
728 and (ii) three thresholds of significance ($-\log_{10} p$-value > 6, $-\log_{10} p$-value > 5, $-\log_{10} p$-value >
729 4).

730 **Identity of candidate genes under directional selection and enrichment in biological**
731 **processes.**

732 To identify pleiotropic candidate genes associated with the 76 evolved eco-
733 phenotypes, we first selected the 50 SNPs the most associated with each evolved eco-
734 phenotype, leading to a total of 3800 SNPs. We then retrieved all the annotated genes located
735 within a 2kb window on each side of those top SNPs, leading to a final list of 4855 unique
736 candidate genes. We finally focused on genes associated with 11 or more evolved eco-
737 phenotypes.

738 To determine which biological processes were important for adaptation of the TOU-A
739 population over eight generations, we tested whether SNPs in the 0.1% upper tail of the F_{ST}
740 value distribution were over-represented in each of 736 Gene Ontology Biological Processes
741 from the GOslim set[63]. 10,000 permutations were run to assess significance using the same
742 methodology as described in Hancock *et al.* (2011)[37]. For each significantly enriched
743 biological process, we retrieved the identity of all the genes containing SNPs in the 0.1%
744 upper tail of the F_{ST} values distribution.

745 ***FLC* haplotypes analysis**

746 Following Li *et al.* (2014)[42], we extracted the 17 SNPs located within *FLC* and we
747 removed from the analysis 44 accessions with more than one missing SNP information. We
748 then merged this data set with the *FLC* SNP data set obtained across 1307 accessions of the
749 Regional Mapping panel project[42,54]. The 17 SNPs data set was used as the input into the
750 software fastPHASE version 1.4.8[64]. fastPHASE was run using the same parameters as

751 described in Li *et al.* (2014)[42] with the exception of invoking the -K20 option to obtain the
752 same number of haplotypes identified in Li *et al.* (2014)[42]. We identified eight haplotypes
753 among the 151 TOU-A accessions. Seventy accessions have a haplotype related to a rapid
754 vernalization response (RV haloptype)[42], whereas 78 accessions have a haplotype related to a
755 slow vernalization response (SV haplotype)[42]. The remaining three accessions are related to
756 an unknown vernalization response profile.
757
758
759 **Data availability.** The raw sequencing data used for this study will be available at the NCBI
760 Sequence Read Archive (http://ncbi.nlm.nih.gov/sra) through the Study
761 accession SRP077483. The phenotypic data that support the findings of this study are
762 available from the authors on a reasonable request. The genomic SNP data files will be
763 archived through the Dryad digital repository upon acceptance for publication.
764
765 **Code availability.** Custom scripts and phenotypic and genomic files used in this study have
766 been archived in a local depository (https://lipm-browsers.toulouse.inra.fr/pub/Frachon2017-
767 NEE/) that can be accessed by the reviewers with the login '**reviewersNEE'** and the
768 password '**FaupKinmyad4**'. All the scripts and data sets will be made available available in
769 the Dryad database upon acceptance of the manuscript. The code for performing genome-
770 wide scan for selection based on temporal differentiation will be made available on the
771 Zenodo database upon acceptance of the manuscript (Vitalis R, Gay L and Navascues M
772 (2016) TempoDiff: a computer program to detect selection from temporal genetic
773 differentiation. INRA. http://dx.doi.org/10.5281/zenodo.375600).
774
775 48. Hamann, A., Wang**,** T., Spittlehouse, D.L. & Murdock, T.Q. A comprehensive, high-

776 resolution database of historical and projected climate surfaces for western North
777 America. *B. Am. Meteorol. Soc.* **94**, 1307 (2013).

778 49. Hendry, A.P. & Kinnison, M.T. The pace of modern life: measuring rates of
779 contemporary microevolution. *Evolution* **53**, 1637-1653 (1999).

780 50. Gingerich, P.D. Rates of evolution on the time scale of the evolutionary process.
781 *Genetica* **112-113**, 127-144 (2001).

782 51. Li, H. *et al.* The sequence alignment/map format and SAMtools. *Bioinformatics* **25**,
783 2078-2079 (2009).

784 52. Koboldt, D.C. *et al.* VarScan 2: somatic mutation and copy number alteration discovery
785 in cancer by exome sequencing. *Genome Res.* **22**, 568-576 (2012).

786 53. Danecek, P. *et al.* The variant call format and VCFtools. *Bioinformatics* **27**, 2156-2158
787 (2011).

788 54. Horton, M.W. *et al.* Genome-wide patterns of genetic variation in worldwide *Arabidopsis*
789 *thaliana* accessions for the RegMap panel. *Nat. Genet.* **44**, 212-216 (2012).

790 55. Zheng, X. *et al.* A High-performance computing toolset for relatedness and Principal
791 Component Analysis of SNP data. *Bioinformatics* **28,** 326-3328 (2012).

792 56. Kang, H.M. *et al.* Variance component model to account for sample structure in genome-
793 wide association studies. *Nat. Genet.* **42**, 348-354 (2010).

794 57. Atwell, S. *et al.* Genome-wide association study of 107 phenotypes in a common set of
795 *Arabidopsis thaliana* inbred lines. *Nature* **465**, 627-631 (2010).

796 58. Hermisson J. & McGregor A.P. Pleiotropic scaling and QTL data. *Nature* **456**, E3-E4
797 (2008).

798 59. Goldringer, I. & Bataillon, T. On the distribution of temporal variations in allele
799 frequency consequences for the estimation of effective population size and the detection

800 of loci undergoing selection. *Genetics* **168**, 563-568 (2004).
801 60. Waples, R.S. A generalized approach for estimating effective population size from
802 temporal changes in allele frequency. *Genetics* **121**, 379-391 (1989).
803 61. Weir, B.S. & Cockerham, C.C. Estimating *F*-statistics for the analysis of population
804 structure. *Evolution* **38**, 1358-1370 (1984).
805 62. Skoglund, P., Sjödin, P., Skoglund, T., Lascoux, M. & Jakobsson, M. Investigating
806 population history using temporal genetic differentiation. *Mol. Biol. Evol.* **31**, 2516-2527
807 (2014).
808 63. The Gene Ontology Consortium. The Gene Ontology project in 2008. *Nucleic Acids Res.*
809 **36**, D440-D444 (2008).
810 64. Scheet, P. & Stephens M. A fast and flexible statistical model for large-scale population
811 genotype data: applications to inferring missing genotypes and haplotypic phase. *Am. J.*
812 *Hum. Genet.* **78,** 629-644 (2006).
813
814

FIGURE LEGENDS

Figure 1 | Genetic variation among accessions and phenotypic evolution between 2002 and 2010. (**a**) Across the six micro-habitats. Genetic variation was detected for the 29 measured phenotypic traits. (**b**) Within each 'soil x competition' micro-habitat. The letters A, B and C stand for the three types of soil. 'w/o *P. annua*' and 'w/*P. annua*' correspond to the absence and presence of *P. annua*, respectively. The number of genetically variable traits varied between 21 (soil A in absence of *P. annua*) and 28 (soil C in presence of *P. annua*). The percentage of evolved genetically variable traits varied between 22.7% (soil C in absence of *P. annua*) and 76.2% (soil A in absence of *P. annua*). Each genetically variable trait (white and colored squares) in a given *in situ* experimental condition was defined as an eco-phenotype (n = 144). The rates of evolution are expressed in *haldanes* (a metric that scales the magnitude of change by incorporating trait standard deviations).

Figure 2 | Phenotypic changes in the TOU-A population over 8 generations. (**a**) Mean phenotypic evolution across the six micro-habitats. The total number of seeds produced can be maintained through evolution of phenological (bolting time and flowering interval) and individual reproductive (seed production on the main stem) traits. (**b**) Comparison among the six *in situ* 'soil x competition' micro-habitats. Average values of the phenotypes differed substantially among the six micro-habitats. (**c**) Evolution within each *in situ* micro-habitat. 'n' indicates the number of evolved phenotypic traits (**Fig. 1**). The identity of genetically variable traits that evolved between 2002 and 2008 depended on the micro-habitat. Each box plot is based on the genotypic values (BLUPs) of the TOU-A accessions (year 2002: n = 80, year 2010: n = 115). (**b**) and (**c**) The letters A, B and C stand for the three types of soil. 'w/o *P. annua*' and 'w/*P. annua*' correspond to the absence and presence of *P. annua*, respectively.

(**a**) and (**c**): solid and dashed boxes indicate significant evolution with absolute *haldanes* > 0.05 and with absolute *haldanes* < 0.05, respectively (**Fig. 1**).

Figure 3 | Genomic patterns of the TOU-A population. (**a**) Hierarchical clustering analysis of the 195 TOU-A accessions and 24 accessions from 10 populations located within 1 km of the TOU-A population. (**b**) Decay of linkage disequilibrium (r^2) with physical distance over the five chromosomes of *A. thaliana*.

Figure 4 | Identification of genomic regions associated with bolting time variation in the TOU-A population. (**a**) Manhattan plots of mapping results for each of the six *in situ* 'soil x competition' treatments. The *x*-axis indicates the physical position along the chromosome. The *y*-axis indicates the $-\log_{10}$ *p*-values using the EMMAX method. MARF > 7%. For each experimental condition, the 200 top SNPs are highlighted in red. (**b**) Venn diagram partitioning the bolting time SNPs detected among the lists of 200 top SNPs for each *in situ* 'soil x competition' treatment. Genetic bases underlying bolting time are largely distinct across micro-habitats

Figure 5 | Genetic architecture underlying *in situ* phenotypic evolution in the TOU-A population when considering a threshold of 200 top SNPs. (**a**) Frequency distribution of the effective number of eco-phenotypes affected by a SNP (N_{eff}, accounting for the correlations among eco-phenotypes)[31] among the 21,268 unique top SNPs. (**b**) Regression of total effect size T_M (total effect size by the Manhattan distance) on N_{eff}. The formula corresponds to the pleiotropic scaling relationship $\boldsymbol{T_M = c^* N_{eff}^{\,d}}$. A scaling component *d* exceeding 1 indicates that the mean per-trait effect size of a given top SNP increased with N_{eff}[3,4]. Solid red line: fitted relationship between T_M and N_{eff}, solid black line: linear

dependence (d = 1). (**c**) Fold-increase in median $-\log_{10}$ (p-values) of neutrality tests based on temporal differentiation for SNPs that hit only evolved eco-phenotypes, only unevolved eco-phenotypes or both types of eco-phenotypes, according to different classes of effective number of eco-phenotypes. The dashed line corresponds to a fold-increase of 1, i.e. no increase in median significance of neutrality tests based on temporal differentiation. (**d**) Fold-increase in median F_{ST} values for SNPs that hit only evolved eco-phenotypes, only unevolved eco-phenotypes or both types of eco-phenotypes, according to different classes of N_{eff} (median F_{ST} across the genome = 0.00293). Significance against a null distribution obtained by bootstrapping: *0.05 > P > 0.01, **0.01 > P > 0.001, ***P < 0.001, absence of symbols: non-significant.

Figure 1

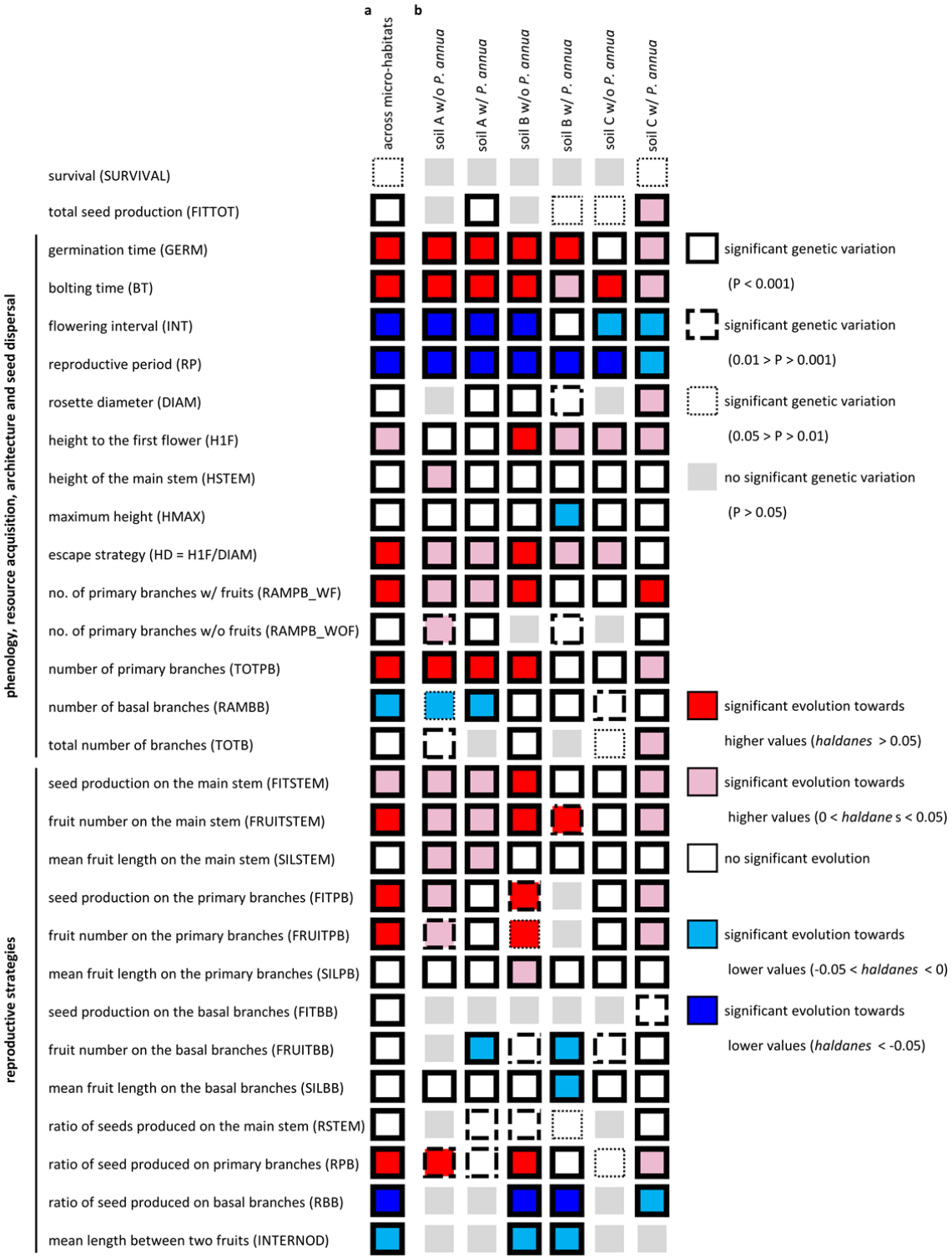
a
b
across micro-habitats
soil A w/o P. annua
soil A w/ P. annua
soil B w/o P. annua
soil B w/ P. annua
soil C w/o P. annua
soil C w/ P. annua
survival (SURVIVAL)
total seed production (FITTOT)
germination time (GERM)
bolting time (BT)
flowering interval (INT)
reproductive period (RP)
rosette diameter (DIAM)
height to the first flower (H1F)
height of the main stem (HSTEM)
maximum height (HMAX)
escape strategy (HD = H1F/DIAM)
no. of primary branches w/ fruits (RAMPB_WF)
no. of primary branches w/o fruits (RAMPB_WOF)
number of primary branches (TOTPB)
number of basal branches (RAMBB)
total number of branches (TOTB)
seed production on the main stem (FITSTEM)
fruit number on the main stem (FRUITSTEM)
mean fruit length on the main stem (SILSTEM)
seed production on the primary branches (FITPB)
fruit number on the primary branches (FRUITPB)
mean fruit length on the primary branches (SILPB)
seed production on the basal branches (FITBB)
fruit number on the basal branches (FRUITBB)
mean fruit length on the basal branches (SILBB)
ratio of seeds produced on the main stem (RSTEM)
ratio of seed produced on primary branches (RPB)
ratio of seed produced on basal branches (RBB)
mean length between two fruits (INTERNOD)
phenology, resource acquisition, architecture and seed dispersal
reproductive strategies
significant genetic variation
(P < 0.001)
significant genetic variation
(0.01 > P > 0.001)
significant genetic variation
(0.05 > P > 0.01)
no significant genetic variation
(P > 0.05)
significant evolution towards
higher values (haldanes > 0.05)
significant evolution towards
higher values (0 < haldane s < 0.05)
no significant evolution
significant evolution towards
lower values (-0.05 < haldanes < 0)
significant evolution towards
lower values (haldanes < -0.05)

877 **Figure 2**

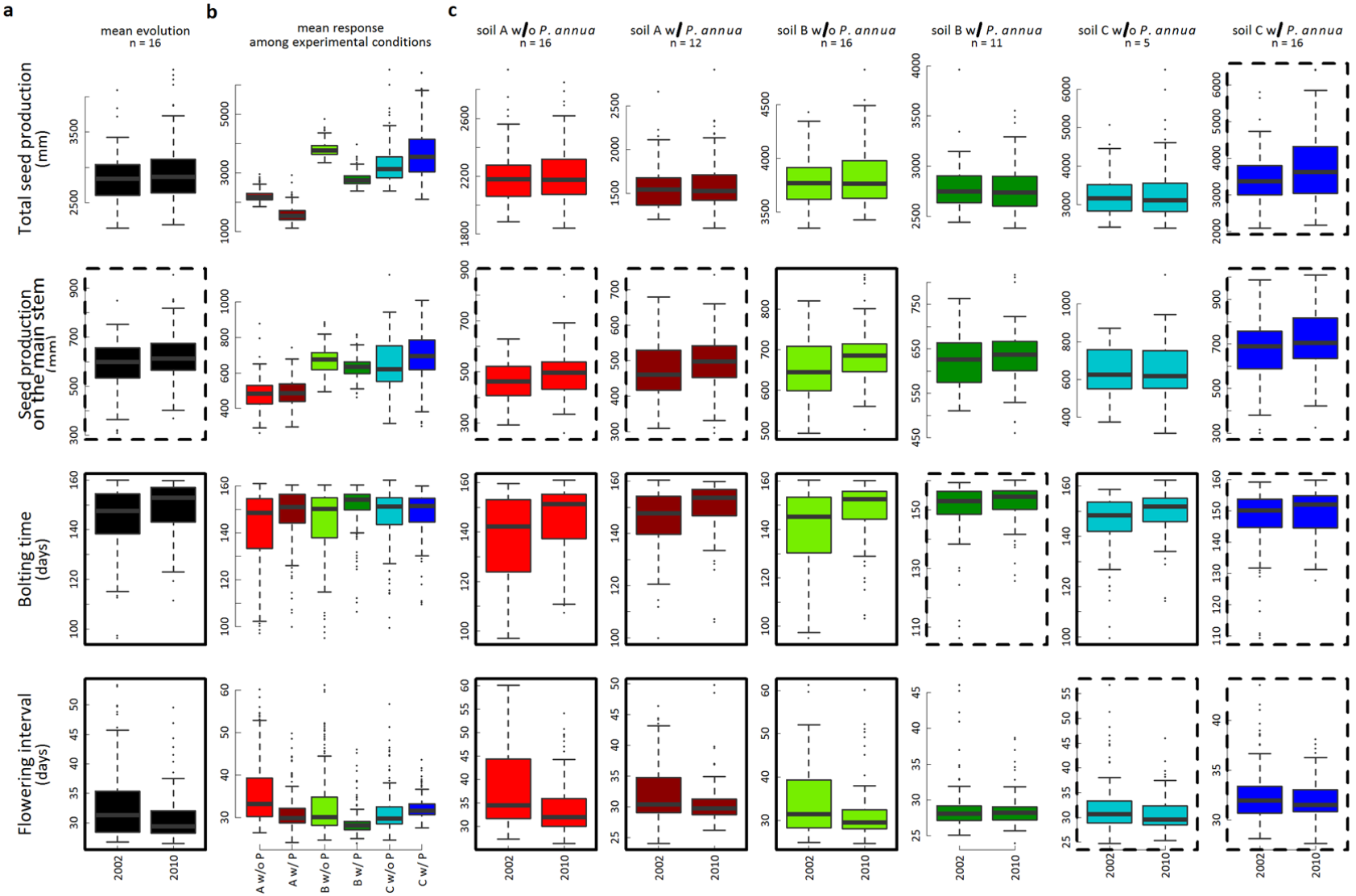

878

Figure 3

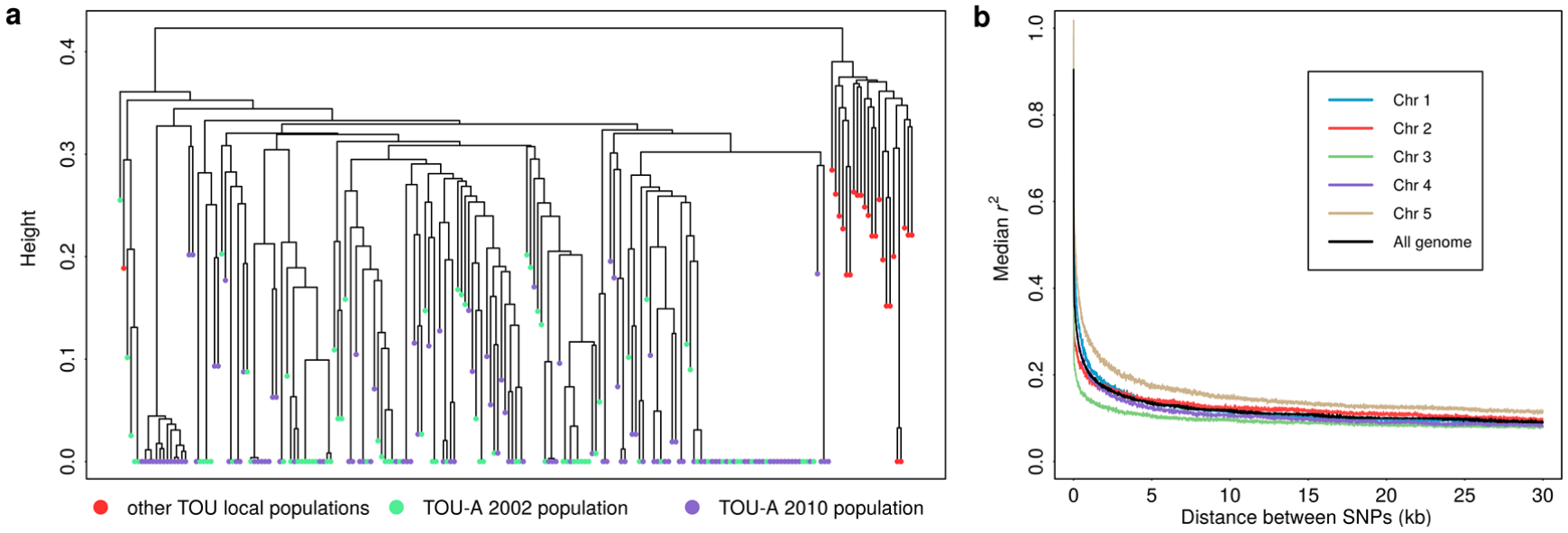
a
Height
0.0
0.1
0.2
0.3
0.4
other TOU local populations
TOU-A 2002 population
TOU-A 2010 population
b
Median r^2
0.0
0.2
0.4
0.6
0.8
1.0
0
5
10
15
20
25
30
Distance between SNPs (kb)
Chr 1
Chr 2
Chr 3
Chr 4
Chr 5
All genome

Figure 4

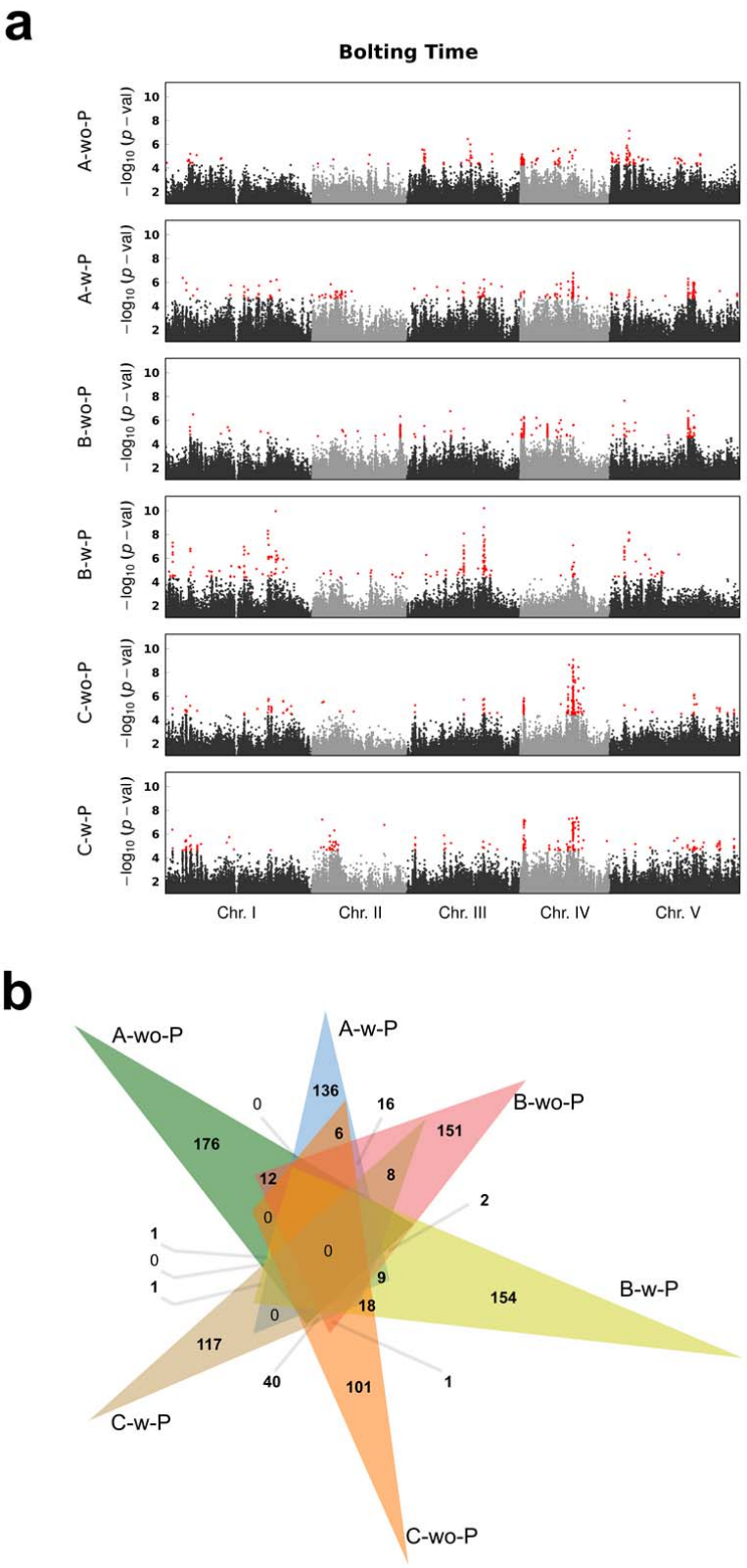
a
Bolting Time
A-wo-P
A-w-P
B-wo-P
B-w-P
C-wo-P
C-w-P
−log10 (p − val)
Chr. I
Chr. II
Chr. III
Chr. IV
Chr. V
b
A-wo-P
A-w-P
B-wo-P
B-w-P
C-w-P
C-wo-P
136
16
176
6
151
12
8
2
0
1
0
1
9
154
18
117
40
101
1

889 **Figure 5**

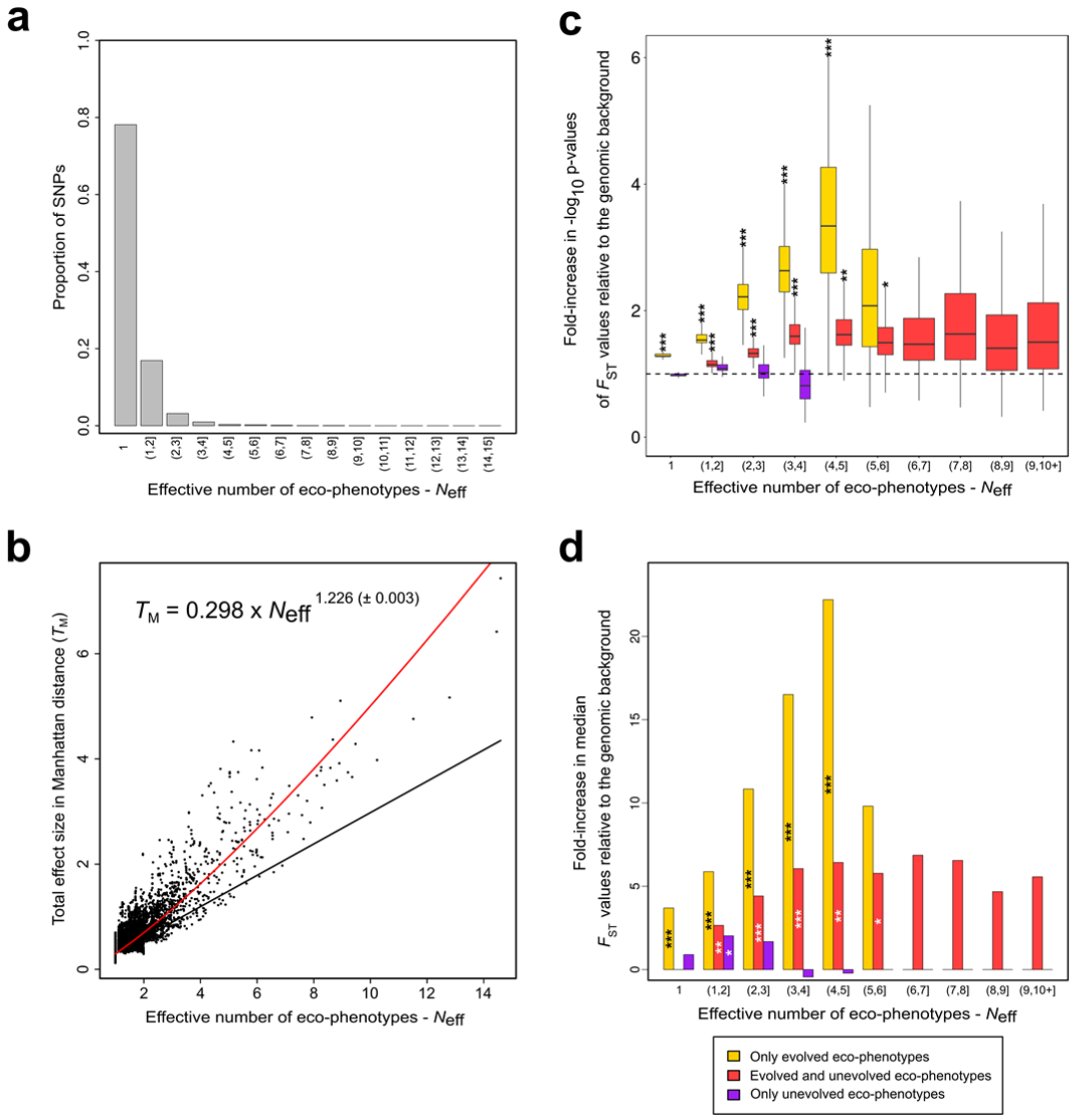

890